Spatial Disparities of Ozone Pollution in the Sichuan Basin Spurred by Extreme Hot Weather

Nan WANG[1*], Yunsong DU[1], Dongyang CHEN[1], Haiyan MENG[1], Xi CHEN[2], Li ZHOU[1], Guangming SHI[1], Yu ZHAN[1], Miao FENG[3], Wei LI[3], Mulan CHEN[4], Zhenliang LI[4], Fumo YANG[1*]

[1]College of Carbon Neutrality Future Technology, Sichuan University, Chengdu, China
[2]Institute of Mass Spectrometry and Atmospheric Environment, Guangdong Provincial Engineering Research Center for On-line Source Apportionment System of Air Pollution, Jinan University, Guangzhou, PR China
[3]Chengdu Academy of Environmental Sciences, Chengdu, 610072, China
[4]Chongqing Research Academy of Eco-Environmental Sciences, Chongqing, 401147, China

Correspondence to nan.wang@scu.edu.cn and fmyang@scu.edu.cn

KEYWORDS: ozone pollution, heatwave, spatial disparity, Sichuan Basin, ozone formation mechanism

Abstract

Under the influence of climate change, the increasing occurrence of extreme weather events, such as heatwaves, has led to an enhanced frequency of ozone (O_3) pollution issues. In August 2022, the Sichuan Basin (SCB), a typical large-scale geographical terrain located in southwestern China, experienced the most severe heatwave over the last 20 years. The heatwave led to substantial disparities in O_3 levels across the region. Here, by integrating observations, machine learnings and numerical simulations, we aim to understand the diverse O_3 formation mechanisms in two mega cities, Chengdu (western location) and Chongqing (eastern location). Observational data showed that Chengdu experienced a consecutive 17-day period of O_3 exceedance, in contrast to Chongqing, where O_3 concentrations remained below the standard. Meteorological and precursor factors were assessed, spotlighting high temperatures, intense solar radiation, and overnight accumulative pollutants as key contributors to O_3 concentrations. The interplay of isoprene, temperature, and O_3, alongside the observation-based box model and MEGAN simulations, underscored the significant role of intensified biogenic VOCs (BVOCs) on O_3 formations. Interestingly, Chongqing exhibited nearly double the BVOCs emissions of Chengdu, yet contributed less to O_3 concentrations. This discrepancy was addressed through CMAQ-DDM simulations and satellite diagnosis by investigating the O_3-NO_x-VOCs sensitivity. Notably, Chengdu displayed a VOCs-driven sensitivity, while Chongqing showed a transitional regime. Moreover, the regional transport also played a pivotal role in the spatial divergence of O_3 pollution. Cross-regional transport predominantly influenced Chongqing (contributing ~80%), whereas Chengdu was mainly affected by the emissions within the basin. The local accumulated pollutants gave rise to the atmospheric oxidizing capacity, resulting in a substantial photochemical contribution to O_3 levels (49.9 ppbv/hour) in Chengdu. This comparison of the difference provides the insights into the complex interplay of meteorology, natural emissions, and anthropogenic sources during heatwaves, guiding the necessity of targeted pollution control measures in regional scales.

1 Introduction

Ground-level ozone (O_3), formed through intricate photochemical reactions involving precursors like volatile organic compounds (VOCs) and nitrogen oxides (NO_x) under sunlight, is a prominent constituent of smog and a major contributor to poor air quality. Different from the protective role in the stratosphere, O_3 in the troposphere has garnered great attention due to its potential damage to human well-being and ecological systems (Krupa and Kickert, 1989; Schwela, 2000; Emberson et al., 2001; Xiao et al., 2021). The hazardous effects span across multiple domains, such as detrimental impact on human health, vegetation growth, and the climate. Addressing O_3 pollution is a complex endeavor, which mainly arises from the nonlinear relationship between O_3 and its precursors. Besides, the substantial influence of meteorological conditions adds another layer of intricacy to the challenge of managing O_3 pollution. Under global warming, the interplay of factors such as extreme weather events and elevated anthropogenic emissions have led to the frequent emergence of O_3 pollution, worsening air quality in urban areas worldwide.

Net O_3 production arises when the equilibrium between O_3 and nitrogen oxides (NO_x), i.e., $NO + O_3 \rightarrow NO_2 + O_2$, is disrupted through the involvement of alkylperoxyl (RO_2) and hydroperoxyl (HO_2) radicals originating from oxidation of VOCs and carbon monoxide (CO). This intervention triggers the oxidation of NO to NO_2, ultimately resulting in the accumulation of O_3 through NO_2 photolysis (Jacob, 2000; Lelieveld and Dentener, 2000). Functioning as a pivotal role in photochemical reactions, VOCs have been identified as a crucial focal point for advancing efforts in the prevention and management of O_3 pollution (Jenkin and Clemitshaw, 2000). However, influenced by the diversity, abundance and reactivity of VOCs species, the spatial and temporal of VOCs characteristics depict regional disparities, adding difficulty in developing an effective strategy to reduce photochemical smog. Moreover, due to the dual roles of NO_x in O_3 formation, where they enhance O_3 formation in low NO_x environments and titrate O_3 in high NO_x environments, reductions in VOCs must be examined along with the patterns of NO_x. Given the diverse energy structures in different regions, comprehending the regional

responsiveness of O_3-NO_x-VOCs sensitivity is essential. This is particularly vital for elucidating non-linear relationship discrepancies within regional contexts, which helps to advance the formulation of effective emission reduction strategies.

O_3 pollution episodes are also closely related to meteorology. High temperature, intensive solar radiation and light winds are found to be the unfavorable weather conditions inducing photochemical pollutions (Ding et al., 2017; Wang et al., 2017; Wang et al., 2022b). Generally, the impact of meteorological conditions on O_3 is manifested through factors such as changes in chemical reaction rates, dry/wet deposition, and atmospheric transport. By objectively classifying pollution weather types, numerous studies have summarized the typical weather conditions that lead to O_3 pollution. For example, high-pressure ridge, continental anticyclone and the periphery of typhoons are the typical weather system conducing O_3 pollutions in east Asia (Mcelroy et al., 1986; Daum et al., 2003; Wang et al., 2015). Besides, meteorology can also indirectly affect O_3 by modulating natural emissions, such as BVOCs (biogenic VOCs) emissions from vegetation and reactive nitrogen emissions from soil (Hall et al., 1996; Saunier et al., 2017; Huang et al., 2018). For instance, a rise in temperature can result in elevated emissions of BVOCs, thereby contributing to the formation of O_3 (Wang et al., 2022b). With the influence of climate change, there is an increasing frequency of extreme weather events, further perturbating the natural emissions and finally exacerbating O_3 pollutions (Lu et al., 2019).

The Sichuan Basin (SCB), encircled by the Qinghai-Tibet Plateau, Yungui Plateau, and surrounding mountain ranges, stands as a notable hotspot for atmospheric pollution within China. Two mega cities, Chengdu and Chongqing, are situated in the SCB with populations exceeding 50 million. In fact, a considerable amount of research on the pollution characteristics of O_3 has been conducted in the SCB. For example, the characteristics of O_3 and the precursors have been widely measured and analyzed (Zhao et al., 2018; Qiao et al., 2019; Zhou et al., 2020; Chen et al., 2022).The complicated coupling effect between the plateau-deep basin topography and the unique meteorological conditions on atmospheric pollution have

been studied (Hu et al., 2022; Shu et al., 2022; Lei et al., 2023). The impact of aerosol feedbacks on O_3 was also explored (Wang et al., 2020).

However, a limited focus has been placed on contrasting the varied responses among different sites or cities within the basin. Exploring and contrasting diverse mechanisms across multiple sites enriches our comprehension and facilitates collaborative air pollution mitigation efforts in a regional scale. In August 2022, the SCB experienced an exceptionally rare heatwave, with monthly mean temperature ranking the highest over the last two decades. As a result, the Chengdu Plain suffered from 17-day consecutive O_3 pollution, whereas Chongqing remained good air quality. Here, we combined field measurements, machine learning and numerical simulations to elucidate the spatial disparities of O_3 pollution mechanism within the SCB. This information has implication for better understanding the meteorological contributions, discrepancy in O_3-NO_x-VOCs sensitivity, and regional transport disparities between large urban areas, and provides insights for regional joint control of O_3 pollution.

2 Method

2.1 Data Source

Data of atmospheric compositions, including O_3, NO_x (NO and NO_2), CO, SO_2, VOCs components and meteorological parameters were collected from two in-situ observational sites. The Chengdu sampling site was located on the rooftop super monitoring station of the Chengdu Environmental Science Academy in Qingyang District, Chengdu (30.65°N, 106.49°E), while the Chongqing sampling site was situated on the rooftop research observation station of Longshan Primary School in Yubei District, Chongqing (29.75°N, 106.46°E). Both sites were situated in mixed-use areas encompassing traffic arteries, commercial, and residential zones, serving as representative locations for assessing urban air quality. Detailed information of the measurements, such as monitoring instruments, data coverage, and resolution were summarized in Table S1. Briefly, the ambient concentrations of O_3, NO_x, CO and SO_2 were detected by instruments produced by Thermo Scientific (Model 49i, 42i, 48i and 43i, respectively). The species of VOCs were sampled by the GC955-611/811

Ozone Precursor Analyser produced by Synspec. The instrument targeted the VOCs species designated as photochemical precursors by the US Environmental Protection Agency (EPA). The gas standards used were identical to those employed by the US EPA Photochemical Assessment Monitoring Stations (PAMS). The photolysis rate of NO2 (JNO2 value) were measured by Ultra-fast CCD-Detector Spectrometer (UF-CCD, MetCon, Germany). Meteorological parameters including temperature, relative humidity, wind speed and wind direction at the same sites were concurrently measured by the mini-weather stations (WS600-UMB in Chengdu and WS502-WTB100 in Chongqing). All instruments were meticulously maintained and regularly calibrated. Moreover, the air quality monitoring network established by the Ministry of Ecology and Environment of China was employed to assess O_3 pollution events in the SCB.

In addition, for regional analysis in this study, we acquired the monthly averaged 90th percentile of MDA8 O_3 (MDA8-90) product. This gridded distributed O_3 product (10×10 km) was reconstructed by integrating surface monitoring, satellite observation, emission inventory, numerical modeling and big data analysis. The data was sourced from TAP (Tracking Air Pollution in China, http://tapdata.org.cn, last accessed on Feb 3, 2024).

2.2 Stepwise Regression Analysis

We employed the stepwise regression analysis to assess the impact of various meteorological factors on O_3 formation. This approach involves the introduction of numerous input variables, with the method iteratively selecting significant factors while eliminating non-significant ones, ultimately resulting in the identification of a final set of critical factors. Following this, we constructed a multivariate linear regression equation to model O_3 concentration. In detail, meteorological parameters were obtained from the fifth generation of the European Centre for Medium-Range Weather Forecasts atmospheric reanalysis (ERA5). The selected parameters included 10m u-component of wind (U10), 10m v-component of wind (V10), vertical wind (w), boundary layer height (BLH), 2m temperature (T2) and surface solar radiation (SSR). Given the high

correlation (R=0.85) between the diurnal variations of T2 and SSR during the heatwave, it was challenging to distinguish the individual impacts of T2 and SSR. As a pragmatic approach, we chose to combine them by multiplying T2 with SSR, thereby examining the collective influence of elevated temperatures and high solar radiation. Additionally, we also incorporated previous night accumulative air pollutants, such as O_3 (ACCO3) and NO_2 (ACCNO2), as input parameters to investigate the impact of pollutants being overnight accumulated on O_3 levels. The machine learning-simulated O_3 concentrations were then validated against observations, revealing a robust correlation (Pearson correlation coefficient (R) > 0.91, p-Value (from two-tailed t-test) < 0.01) between them (Fig S1). This result demonstrates the effectiveness of meteorological and overnight accumulative factors in explaining a substantial portion of O_3 concentrations.

2.3 Observation-based model (OBM)

In this study, an observation-based box model (OBM) configured with the master chemical mechanisms (MCM v3.3.1) was employed to identify the key VOCs species influencing O_3 (Jenkin et al., 2015; Bloss et al., 2005; Saunders et al., 2003; Jenkin et al., 2003; Jenkin et al., 1997). The model considered VOCs concentrations, trace gases (O_3, NO_x, CO, SO_2), meteorological parameters, as well as the photolysis rates of NO_2 (J_{NO_2}) from the in-situ sites in Chengdu and Chongqing. Observations were used as constraints in the model and were averaged to represent the diurnal cycle with a time resolution of 1 hour. The photolysis rates generated by the model were adjusted based on the measured J_{NO_2} values in order to accurately simulate the photochemical reactions. The mean mixing ratios of 46 VOCs species, including 20 alkanes, 11 alkenes, 1 alkyne (ethyne) and 14 aromatics were listed in Table S2. The model started at 00:00 local time (LT) and ran for a period of 24 hours. Prior to the formal calculation, we conducted a spin-up run for 4 days with constraints representing the diurnal cycle, allowing the unconstrained compounds (e.g., radicals and HCHO) to reach steady states. Using the OBM simulation, the relative incremental reactivity (RIR) method was applied to assess the sensitivity of O_3 formation to individual precursor species (Cardelino and Chameides,

1995; Meng et al., 2023; Zhang et al., 2019; Xue et al., 2014; Zhu et al., 2020). The calculation process can be expressed in Eq. (1).

$$\mathrm{RIR}(X)=\frac{(\mathrm{P}_{\mathrm{O}_3}(X)\text{-}\mathrm{P}_{\mathrm{O}_3}(\Delta X))/\mathrm{P}_{\mathrm{O}_3}(X)}{\Delta \mathrm{C}(X)/\mathrm{C}(X)} \quad (1)$$

Here, X represents a specific precursor of O_3. $\mathrm{P}_{\mathrm{O}_3}(X)$ and $\mathrm{P}_{\mathrm{O}_3}(\Delta X)$ represent the maximum simulated O_3 concentration based on measured concentration and the concentration when the precursor levels change by ΔX. $\Delta \mathrm{C}(X)/\mathrm{C}(X)$ indicates the relative change of precursor X. In this study, a reduction of 20% in precursor X was selected to perform the RIR analysis.

2.4 Lagrangian Particulate Dispersion Modeling

We conducted backward Lagrangian particulate dispersion modeling (LPDM) to ascertain the potential source regions for the air masses observed at the monitoring stations. This approach involved employing the hybrid single-particulate Lagrangian-integrated trajectory model (HYSPLIT) driven by the ARL format Global Data Assimilation System (GDAS) data. The LPDM was executed with a temporal resolution of 1 hour, releasing 3000 particulates at 100 meters above sea level from the site and then tracking their backward movement for 72 hours. The particulates' positions were calculated in both vertical and horizontal dimensions, considering the impact of atmospheric advection and diffusion. By analyzing the resulting data, we derived the "retroplume", which indicates the spatial residence time of particulates and reflects the distribution of surface probability or simulated air mass residence time. This technique enabled us to diagnose whether the in-situ observation was predominantly influenced by local emissions or regional transport.

2.5 Chemical transport modeling

A chemical transport model, WRF-MEGAN-CMAQ (Weather Research Forecast – Model of Emissions of Gases and Aerosols from Nature – Community Multiscale Air Quality), was employed to study the O_3 formation mechanism in the SCB. We adopted a two-nested domain, with the outer domain covering most parts of east Asia (grid resolution of 36×

36 km) and the inner domain covering the southwestern China with the SCB being focused (grid resolution of 12×12 km) (see Fig S2). The European Center for Medium-Range Weather Forecasts (ECMWF) reanalysis data was used as the initial and lateral boundary conditions of the WRF (version 3.9.1). Carbon Bond Mechanism Version 6 and Aerosol Scheme 6 were used for gas-phase and aerosol chemical simulations within the CMAQ model (version 5.4), respectively. With regard to anthropogenic emissions, the recently updated 2020-based MEIC emissions (Multi-resolution Emission Inventory for China, developed by Tsinghua University) were used for areas within China and the 2010-based MIX emissions (Li et al 2017) were used for regions outside China. Both sets of the emissions have a horizontal resolution of 0.25×0.25°, incorporating sectors such as transportation, industry, power plant, residential and agriculture. Besides, natural emissions were calculated using MEGAN model (version 2.1) driven by the WRF simulated meteorology. The static input vegetation-related data of MEGAN were updated by using the 2020-based the plant function type (PFT) and leaf area index (LAI) retrieved from the MODIS (Moderate-Resolution Imaging Spectroradiometer) products. After a spin-up of 5 days, the WRF-CMAQ model was performed to simulate O_3 concentrations in the SCB. More details of the modeling configuration were summarized in Table S3.

In this study, we introduced the CMAQ-DDM (Decoupled Direct Method) module to investigate the non-linear relationship between O_3 and its precursors. Unlike the traditional brute force method (BFM) that involves cutting or eliminating emissions from source regions (or sectors), which is not only computationally intensive but also prone to uncertainties (due to the intricate non-linear nature of O_3 chemistry), the DDM method offers a more refined alternative. It enables accurate and computationally efficient calculations of the sensitivity coefficients required for evaluating the impact of parameter variations on output chemical concentrations (Napelenok et al., 2008). Furthermore, the DDM method has been reported to exhibit more accurate calculations when addressing uncertainties arising from the nonlinear relationship between secondary pollutants and their emissions, in comparison to the BFM (Itahashi et al., 2015). Herein, both

first-order and higher order sensitivities were calculated to obtain the O_3–NO_x–VOCs sensitivities in Chengdu and Chongqing. In addition, we also utilized the CMAQ-ISAM (Integrated Source Apportion Method) technique, an innovative approach for source tracing. This method enables us to trace and quantify the distinct impacts on O_3 concentrations originating from specific source sectors, emissions confined within designated geographical regions, as well as effects arising from stratospheric and lateral boundary conditions (Kwok et al., 2013). Through this approach, we calculated the separate influences of anthropogenic and biogenic emissions on O_3 levels. We also assessed the contributions of source regions to O_3 levels in Chengdu and Chongqing, encompassing both local and regional influences. A map of source region's classification in this study was provided in Fig S3.

We validated the performance of the WRF-MEGAN-CMAQ model using surface network monitoring data. The time series and statistical outcomes of the simulated and observed O_3 within the SCB are consolidated in Fig S4 and Table S4. In general, the favorable alignment between observations and simulations underscores the model's proficiency in accurately replicating the magnitude and temporal variations of air pollutants.

3 Results and discussion

3.1 Regional disparity of O_3 between Chengdu and Chongqing
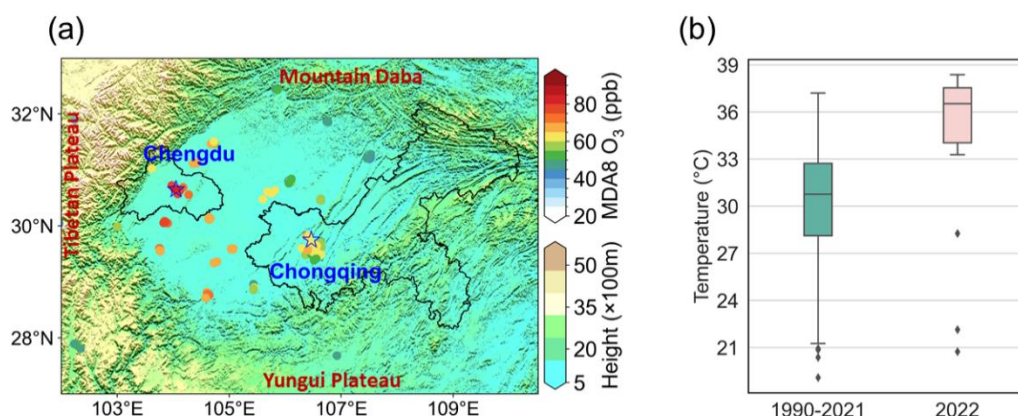
Fig 1 (a) Geographical distribution of Sichuan Basin with scattered averaged monthly MDA8 O_3 concentrations (data obtained from Ministry of Ecology and Environment of China). The contoured shows the 3D terrain height in SCB. The black lines highlight the administrative

 (b) Historical monthly averaged daily-maximum air

309 temperature (August) comparison between 2022 and climate average (1990-2021) of the SCB

310 region.

311 August 2022 witnessed the SCB experiencing its hottest August in the last
312 20 years, with Chengdu and Chongqing reporting monthly mean
313 temperatures soaring to 36.8°C and 40.3°C, respectively (Fig 1). Typically,
314 the atmospheric conditions in the SCB are relatively stable due to the
315 topography of the basin. This stability, in conjunction with elevated
316 temperatures, tended to foster the occurrence of photochemical pollution
317 (Zhao et al., 2018; Chen et al., 2022). However, during this historically
318 unprecedented heatwave, O_3 levels exhibited substantial variations across
319 the SCB. Observations revealed that O_3 concentrations surpassed China's
320 Grade II standard (75 ppbv) in the western part of the SCB, notably in
321 Chengdu. Conversely, significantly lower concentrations, well below the
322 standard, were observed in the eastern region of the basin, particularly in
323 Chongqing (Fig 1a). According to the network monitoring data, the average
324 maximum daily 8-hour (MDA8h) O_3 concentration in Chengdu was
325 measured at 75.1 ppbv. In contrast, the MDA8h O_3 concentration in
326 Chongqing was recorded at 55.1 ppbv.
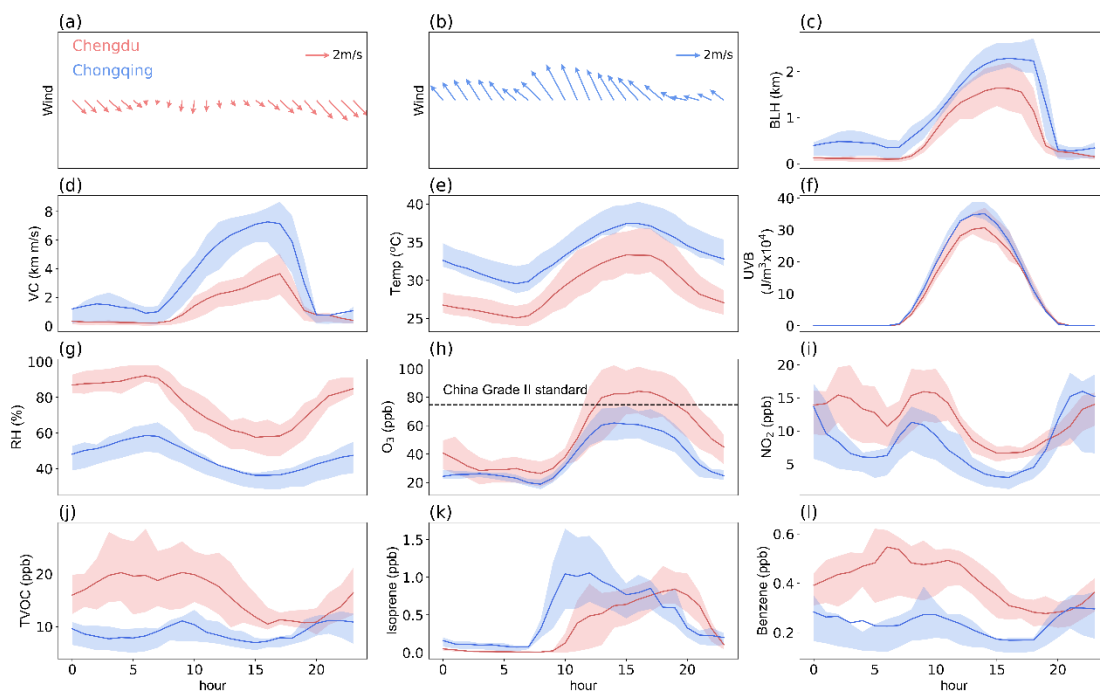
327

328 Fig 2 Diurnal variation of meteorological parameters (including winds, boundary layer height

(BLH), ventilation coefficient (VC), temperature (temp), ultraviolet radiation (UVB) and relative humidity (RH)) and air pollutants (O_3, NO_2, total volatile organic carbons (TVOC), isoprene and benzene) in Chengdu and Chongqing, respectively.

We compared the averaged diurnal variations of the in-situ measured meteorological parameters and air pollutants (Fig 2). Consistent with the analysis of weather patterns, Chongqing was influenced by the southeast winds (3.1 m/s), while Chengdu was more stagnant with lighter wind speed (1.4 m/s) (Fig 2a-b). In addition, the boundary layer height (BLH) was also significantly higher in Chongqing (Fig 2c). A simple calculation of the ventilation coefficient (VC) with wind speed and BLH indicated that Chongqing (VC=3.34 km·m/s) had better ventilation conditions compared to Chengdu (VC=1.24 km·m/s, Fig 2d). It could be inferred that, influenced by lighter winds and lower BLH, air pollutants in Chengdu were more easily trapped and accumulated. Both cities displayed typical meteorological features of a heatwave conducive to photochemical pollution, characterized by elevated temperatures, intense solar radiation, and low relative humidity (Fig 2e-2g). Among these factors, temperature and solar radiation in were higher compared to those in Chengdu, suggesting that the conditions in Chongqing were more conducive to photochemical O_3 reactions. Additionally, significantly lower relative humidity was observed in Chongqing, suggesting a potential reduction in O_3 removal by water vapor, for instance, through HO_x reactions. However, the degree of O_3 pollution was quite the opposite as previously mentioned (Fig 1a and Fig 2h). We conducted further investigation into the diurnal variation of the precursors. Two distinct peaks in NO_2 levels were identifiable, with one occurring in the morning and the other appearing during night (Fig 2i). The morning peaks were likely influenced by vehicular emissions during rush hours. The night peaks were possibly caused by the NO_x titration effect. Moreover, the levels of total VOCs (TVOC) were much higher in Chengdu than those in Chongqing (Fig 2j). Considering the different degrees of NO_2 and TVOC concentrations in Chengdu and Chongqing, it could be inferred that there might be differences in the O_3 formation mechanism between the two cities. Indeed, the diurnal variation of isoprene, a highly active VOCs compound, showed distinct differences (Fig 2k). The observed data in Chongqing showed a

notable afternoon peak, whereas in Chengdu, the peak appeared exclusively between 17:00 and 20:00. Usually, isoprene, mainly emitted by vegetation, is sensitive to ambient temperature and solar radiation and peaks at noon time. There might be some potential explanations. Firstly, the isoprene peak between 17:00 and 20:00 in Chengdu could be attributed to other sources, such as vehicular emissions. However, this possibility was ruled out after examining the diurnal variation of benzene (Fig 2l). As a marker of anthropogenic vehicular emissions, benzene did not exhibit any peaks between 17:00 and 20:00. The second possibility was that the atmospheric oxidizing capacity in Chengdu was more robust than in Chongqing, leading to the rapid photochemical consumption of isoprene emitted by vegetation. This hypothesis was supported by the diurnal variations in O_3 levels, which were notably elevated in the afternoon, implying of a stronger atmospheric oxidizing capacity. The instrument-detected of isoprene was indicative of its "aged" state, implying the rapid photochemical consumption due to both the atmospheric oxidizing capacity and the inherent reactivity of isoprene itself. Furthermore, a distinct decrease of BLH between 17:00 and 20:00 was also a possible reason causing the isoprene peak of Chengdu in the late afternoon.

Subsequently, we employed a machine learning method, the Stepwise Regression Analysis, to quantify the impact of diverse meteorological parameters and precursor concentrations on O_3 levels. In both cities, the significance of T2 and SSR, along with ACCO3 and ACCNO2, took precedence. This indicates that meteorological conditions characterized by high temperatures, intense solar radiation, and the presence of overnight accumulative pollutants played a pivotal role in O_3 concentration, especially during heatwaves. The distinction between the two cities lied in the significance of atmospheric dispersion capacities represented by the variations in winds and BLH. The study revealed that winds, including both horizontal winds (U10 and V10) and vertical wind (W), along with BLH, had positive effects in elevating O_3 levels in Chengdu. Conversely, they predominantly had negative effects, resulting in a decrease in O_3 levels, in Chongqing. These findings align with the diurnal analysis, which indicated that Chengdu experienced lighter winds and lower BLH. The poor

ventilation conditions facilitated the accumulation of air pollutants, contributing to the increase in O_3 levels. In contrast, the ventilation condition in Chongqing was conducive to reduce O_3 concentrations. Combined with the aforementioned analysis of diurnal patterns, it could be inferred that Chengdu was more constrained by local emissions, while Chongqing was more susceptible to regional transport influences (further discussed in Section 3.3).
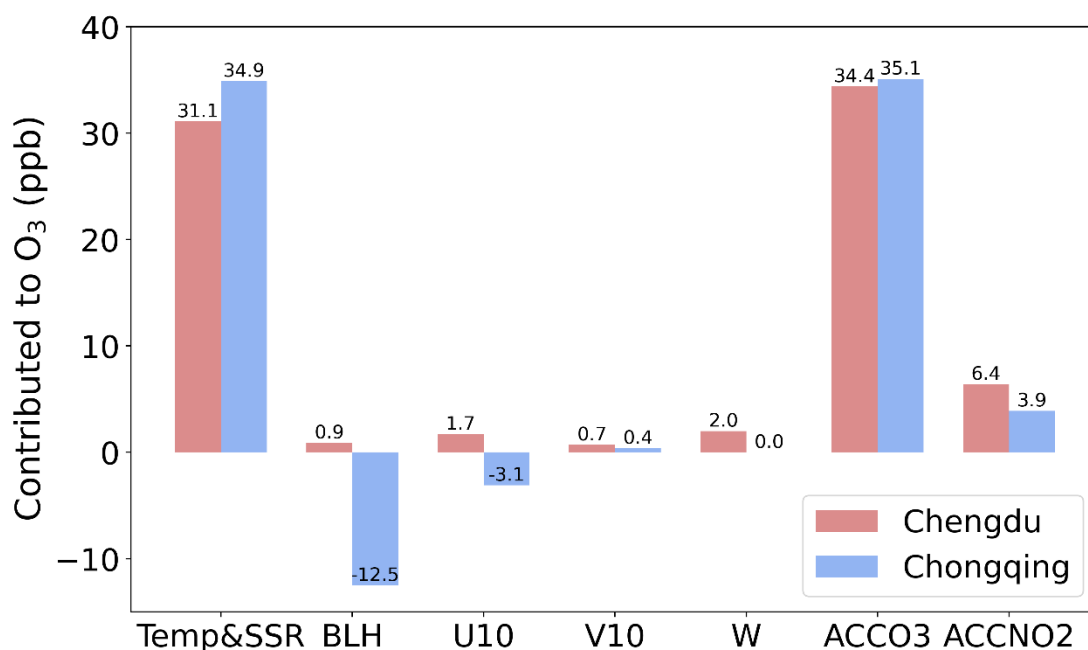
Fig 3 Contribution of multi-factors influencing O_3 concentrations in Chengdu and Chongqing, respectively. (Temp, SSR, BLH, U10, V10, W, ACCO$_3$ and ACCNO$_2$ stand for temperature, surface solar radiation, boundary layer height, 10 m u-component of wind, 10 m u-component of wind, vertical wind, previous night accumulative O_3 and previous night accumulative NO_2, respectively)

3.2 Difference in heatwave-intensified BVOCs emissions and their impact on O_3 formation

In addition to the influence of meteorological factors under heatwave conditions, the precursors also play important roles in contributing O_3 concentrations. Therefore, we utilized the OBM model to compute and identify the primary VOCs components that exerted a substantial influence on O_3 levels. Here, we introduced the RIR values that could reflect the importance of a given species to O_3 concentrations. As Fig 4 shows, Alkenes and aromatic hydrocarbons were the principal VOCs components

influencing O_3 levels in both cities. In Chengdu, the most influential VOCs species on O_3 concentrations included isoprene, m-xylene, trans-2-butene, o-xylene, cis-2-butene, toluene, ethene, 1-hexene, 1,2,4-trimethylbenzene, and 1,2,3-trimethylbenzene. Similarly, in Chongqing, the primary VOCs contributors to O_3 levels were isoprene, m-xylene, trans-2-butene, cis-2-butene, o-xylene, 1,2,4-trimethylbenzene, trans-2-pentene, propane, cis-2-pentene, and toluene. According to the results, both Chengdu and Chongqing should prioritize the regulation of alkenes and aromatic hydrocarbons from sources like vehicular emissions and solvent usage. Besides, the results clearly highlight isoprene as the dominant VOCs species impacting O_3 levels. The characteristics of the heatwave were high temperature, intense solar radiation and dry air condition. These meteorological factors significantly enhanced the emission of BVOCs from vegetation, indicating the notable role of heatwave-triggered natural emissions in the secondary O_3 pollution.
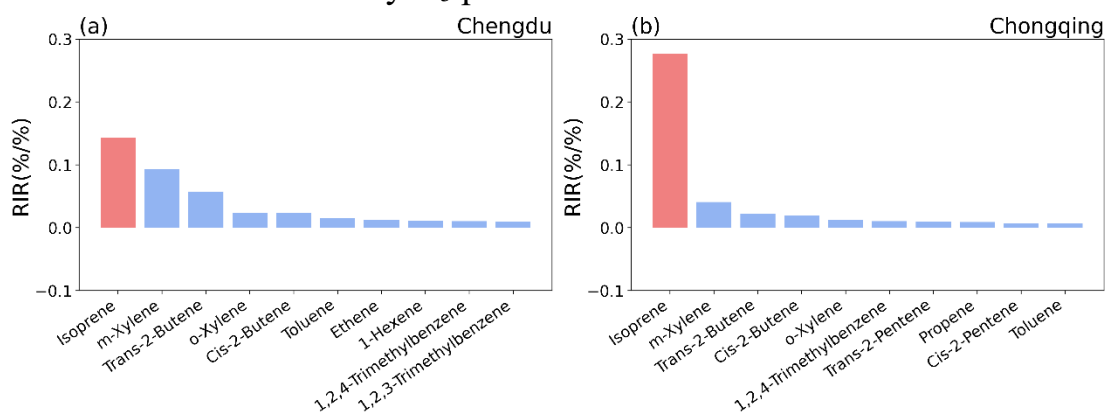
Fig 4 OBM calculated the top 10 VOCs species with the highest RIR values in (a) Chengdu and (b) Chongqing, respectively.

We further examined the relationship between isoprene, temperature, and O_3 using observational data. In order to expand the sample size, we gathered a dataset corresponding to the daily maxima O_3 values recorded during the months of July and August in 2022. In Chengdu, the variations of isoprene and temperature basically showed an increasing trend, indicating that higher isoprene concentrations were associated with higher temperatures, which in turn coincided with elevated O_3 levels (Fig 5a). In Chongqing, the concentration of isoprene initially increased with rising temperatures. However, when the temperature surpassed approximately 40°C, the isoprene concentration started to decrease with further

temperature elevation (Fig 5b). Notably, the peak values of O_3 corresponded closely to the high values of isoprene, occurring at temperatures ~ 38°C to ~ 42°C. According to recent studies, isoprene emissions increase with rising temperatures, and even under high-temperature conditions when vegetation closes stomata, due to the indirect impact of elevated leaf temperature, it decreases only under extreme high-temperature drought conditions because of the inhibition of substrate supply (Potosnak et al., 2014; Wang et al., 2022a). Here, the variation of isoprene with temperature in Chengdu and Chongqing illustrates these two distinctions though the isoprene concentration being observed was "aged".
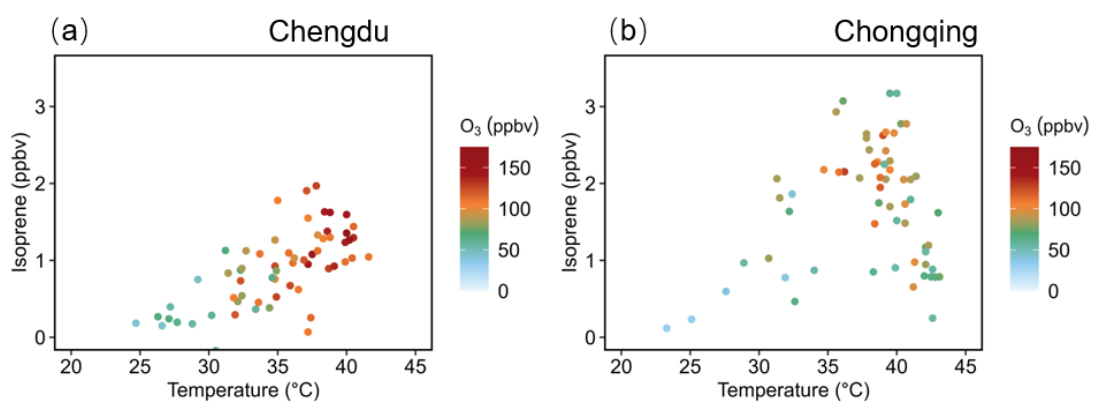
Fig 5 Scatter plots of observed isoprene, temperature and O_3 in (a) Chengdu and (b) Chongqing. The data were collected corresponded to daily maxima O_3 concentrations from July 2022 to August 2022.

We utilized the theoretical calculation from MEGAN model to quantify the disparities in isoprene emissions between the two cities. Considering the varying administrative areas of Chengdu (14,378 km²) and Chongqing (82,339 km²), comparing the total isoprene emissions might not be appropriate. Instead, we quantified the emissions per unit grid area (9×9 km) for both locations (Fig 6). We used two sets of meteorological fields to drive the MEGAN model. One set corresponded to the meteorological fields simulated by WRF for the summer of 2021, while the other set corresponded to the meteorological fields simulated by WRF for the summer of 2022. Among these, the BVOC emissions obtained by driving the MEGAN model with the meteorological fields from the summer of 2021 were considered as ISOP emission by base meteorology (BaseMETE). The difference in BVOC emissions obtained by driving the

MEGAN model with the meteorological fields from the summer of 2022, compared to Base METE, was considered as ISOP emission induced by heatwave (ByHeatwave). It ccould be observed that the isoprene emissions in Chongqing were higher than those in Chengdu (nearly twice as much). In particular, under the influence of heatwaves, the isoprene emissions in Chongqing and Chengdu increased by 41.1% and 22.2%, respectively. The significant role of heatwave-intensified BVOCs emissions was expected to aggravate O_3 pollution in Chengdu and Chongqing. With the aid of CMAQ-ISAM simulation, we proceeded to quantify the distinct impacts of anthropogenic emissions and BVOCs emissions on O_3 concentrations. The findings indicated that at 13:00 (local time), when photochemical reactions were most intense, anthropogenic emissions contributed to 50.6 ppbv and BVOCs emissions contributed to 33.3 ppbv in Chengdu. In comparison, anthropogenic emissions and BVOCs emissions contributed to 31.3 ppbv and 20.6 ppbv in Chongqing, respectively. Interestingly, despite higher BVOCs emissions in Chongqing compared to Chengdu, the contribution of BVOCs to O_3 levels was actually smaller in Chongqing than in Chengdu. This implies that there were differences in the O_3-NO_x-VOCs response mechanisms between the two cities.
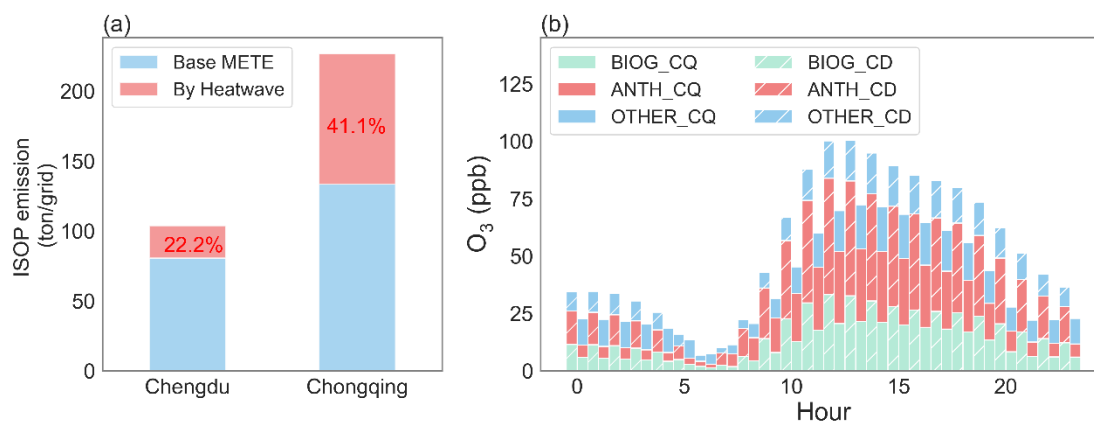
Fig 6 (a) Meteorology driven ISOP emission between Chengdu and Chongqing, respectively.; (b) Averaged source contributions (by emissions) to diurnal O_3 levels in Chengdu (CD) and Chongqing (CQ), respectively. BIOG, ANTH and OTHER refer to contributions from the biogenic, the anthropogenic and the others.

Herein, we conducted CMAQ-DDM simulations to investigate the nonlinear relationship between O_3 and its precursors. Indeed, the O_3-NO_x-

VOCs sensitivity response mechanisms in Chengdu and Chongqing were of difference (Fig 7 a-b). On the one hand, the Chengdu region demonstrated a greater sensitivity (first-order sensitivity coefficients) to VOCs in comparison to Chongqing. Specifically, in certain urban grids within Chengdu, the sensitivity coefficient exceeded 10 ppbv, while the highest sensitivity in Chongqing was only ~ 3 ppbv. On the other hand, Chongqing generally exhibited higher sensitivity to NO_x, except for quite limited urban cores. In contrast, the eastern areas of Chengdu, particularly its urban cores, displayed low sensitivity to NO_x. Furthermore, by taking both the first-order sensitivity coefficient and the 2nd-order sensitivity coefficient into account, we constructed the O_3 isopleth for both cities during the month of August (Fig 7 c-d). It was evident that Chengdu was situated in a VOCs-limited regime, while Chongqing was operating within a mixed-limited regime. These simulated results agree with the satellite diagnosed O_3 formation sensitivity (obtained through the ratio of HCHO and NO_2), confirming again the good modeling performance (Fig S5). The results implied that a temporary decrease in NO_x emissions in Chengdu would result in an increase in O_3 concentrations, whereas reducing VOCs emissions could potentially lower O_3 pollution. This finding could partially explain the increasing trend of O_3 concentrations in Chengdu Plain during the past as the previous emission control measures were mainly targeted to NO_x emissions (driven by the need to control acid rain and $PM_{2.5}$ pollution, successively). In Chongqing, differently, a reduction in either NO_x emissions or VOCs emissions could contribute to alleviating O_3 pollution. The disparity in O_3-NO_x-VOCs sensitivity between the two cities could also elucidate the reason why Chongqing, despite its higher BVOCs emissions, exhibits a lower contribution to O_3 levels. Considering the varying regional sensitivities in O_3-NO_x-VOCs formation, it is advisable to implement precise emission reduction strategies tailored to the unique sensitivities of each city for effective pollution prevention and control. This approach stands in contrast to a uniform solution that may not suit all contexts. For example, in Chengdu, the previously nationally implemented strategy, which prioritized NO_x-focused control, might ultimately lead to O_3 reduction through substantial NO_x reductions. However, this approach

536 would initially enter into a phase characterized by relatively high O$_3$
537 concentrations (positioned within the transitional regime based on the O$_3$
538 isopleth), posing environmental risks. Instead, a strategy centered on VOCs
539 control alongside simultaneous NO$_x$ control could bypass the "high-O$_3$"
540 phase and align with the need to address both O$_3$ and PM$_{2.5}$ pollution.
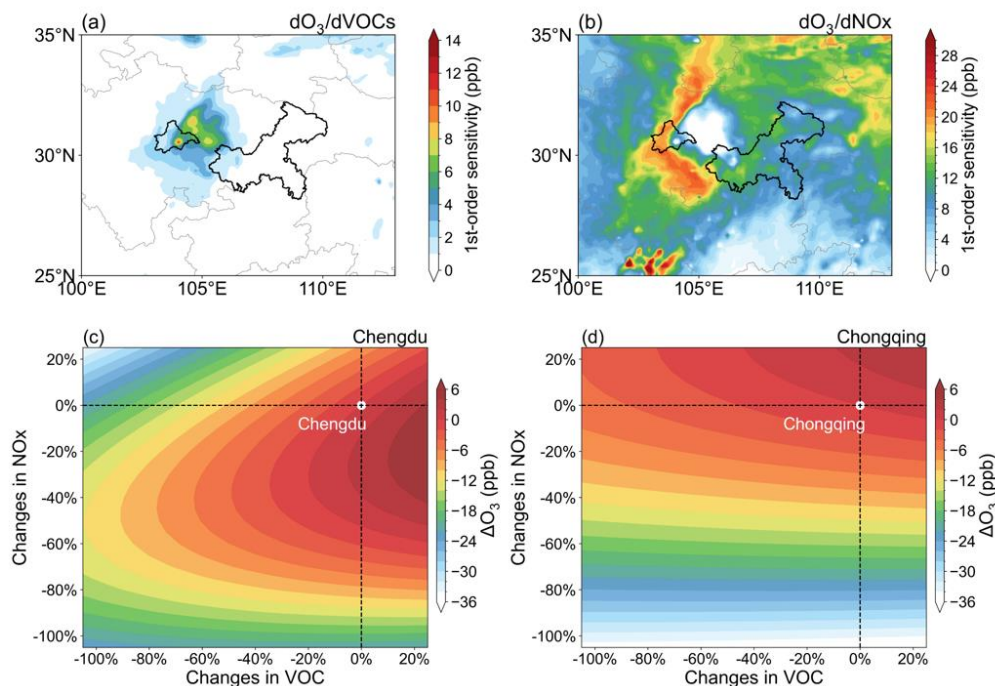
542 Fig 7 Spatial distribution of daytime first-order sensitivity coefficients to (a) VOCs and (b)
543 NO$_x$; O$_3$ isopleth plots in (c) Chengdu and (d) Chongqing

3.3 Regional divergence of source region contribution

545 Surface-level O$_3$ concentrations are influenced not only by photochemical
546 reactions but also by regional transport. In this section, we mainly focus on
547 the disparities in the impact of regional transport on O$_3$ between Chengdu
548 and Chongqing.

549 The distribution of O$_3$ concentration in China's southwestern region, as
550 shown in Fig 8a, revealed that high O$_3$ concentrations were mainly
551 concentrated in the SCB region. In contrast, the O$_3$ concentration in the
552 adjacent Yunnan-Guizhou Plateau (southeast) was very low, indicating a
553 poor-O$_3$ region. According to the synoptic flows, it could be seen the
554 prevailing wind was southeastward, and the wind speed gradually
555 decreased from east to west, implying that Chengdu was more stationary
556 than Chongqing. Our LPDM-simulated 72h backward retroplumes (Fig 8b)

showed that, Chengdu was primarily influenced by local air masses encompassing areas such as Chengdu city and the eastern parts of the SCB. Relatively fewer air masses originated from cross-province transport in the southeast direction. The distribution of NO_x emissions showed that Chengdu was significantly influenced by the locally anthropogenic emissions. Differently, Chongqing showed a situation to be more susceptible to cross-regional transport influences. The dominant air masses in Chongqing not only originated locally but also experienced cross-province transport from the southeast, influenced by the regions such as Yungui Plateau, a poor-O_3 region with relatively low anthropogenic emissions but high BVOC emissions. Considering the strong reactivity and limited lifetime of BVOCs, their role on downwind air quality is rather limited. To support this, we adopted CMAQ-ISAM to identify the local and non-local O_3-precursors with their relative contribution to O_3 concentrations in both cities (see discussions below). The LPDM simulation result was consistent with the synoptic analysis in Fig S6. By examining the difference between 2022 Aug and climate average (1990-2021), it was found that the anomalies of high air temperature and low relative humidity were connected with the strong-southerly-driven cross-regional transport of cool and relatively clean air masses from the Yungui Plateau, which could suppress the photochemical O_3 production in Chongqing. In contrast, Chengdu experienced a typical stationary condition with light wind, high temperature and low relative humidity, which were conducive to local photochemical pollution.

Besides, we also adopted the in-situ measured data by comparing the ratio of m, p-xylene and ethylbenzene. Given that m, p-xylene is more reactive than ethylbenzene, their ratios typically decrease due to photochemical reactions that take place during the transport of air masses. As shown in Fig S7, the ratio was much lower in Chongqing (1.04 ppbv ppbv^{-1}), indicating the presence of "aged" air masses being monitored. Conversely, a higher ratio (3.11 ppbv ppbv^{-1}) in Chengdu indicated the prevalence of "fresh" air masses likely originating from local emissions. The discovery reaffirmed that Chongqing exhibited superior ventilation conditions compared to Chengdu. This inference suggests that Chongqing's enhanced

dispersion capacity played a pivotal role in significantly reducing its O_3 concentrations during the severe heatwave period.
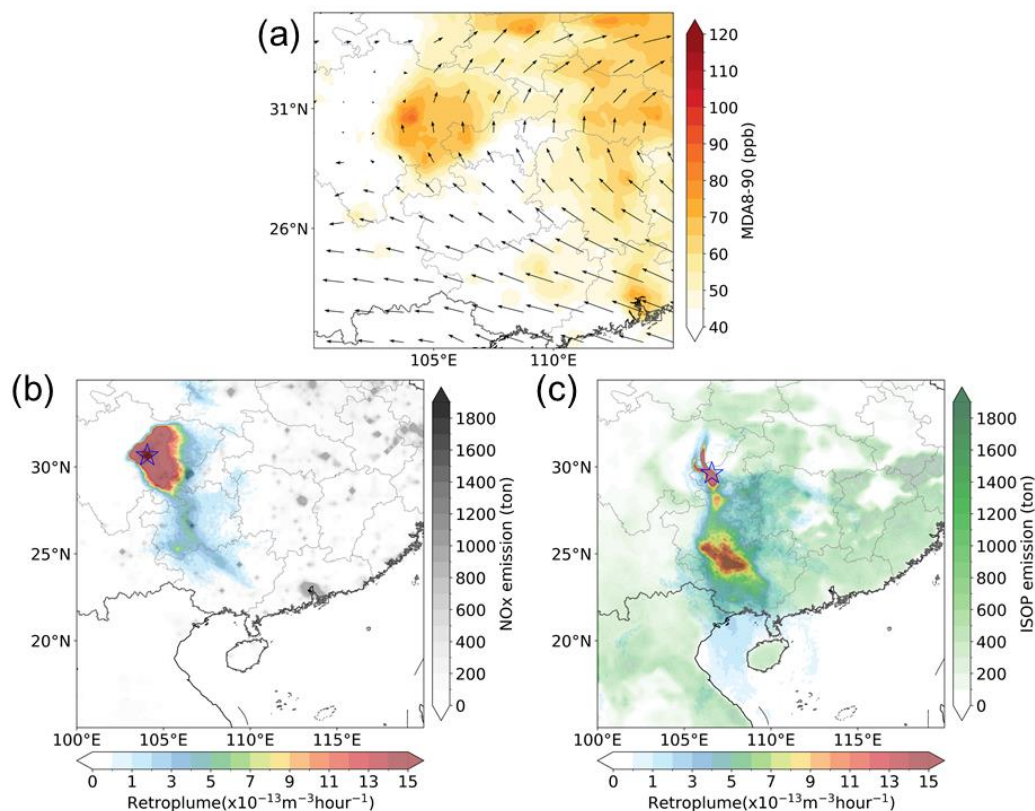
Fig 8 (a) Distribution of monthly averaged 90th percentile of MDA8 O_3 (MDA8-90, TAP dataset) concentrations and monthly averaged winds at 500hPa; (b) 72h retroplume (footprint residence time) showing transport pathways of air masses arriving at Chengdu, and distribution of anthropogenic NO_x emissions; (c) 72h retroplume (footprint residence time) showing transport pathways of air masses arriving at Chongqing, and distribution of biogenic isoprene (ISOP) emissions in August 2022

Further, we employed the CMAQ-ISMA modeling system to quantify the source region's contribution to Chengdu and Chongqing (Fig 9). In this study, we divided the study area into eight major regions, namely Chengdu Plain (CD Plain), Chongqing (CQ), South Sichuan (South SC), Northeast Sichuan (Northeast SC), Northwest Region (Northwest), Southwest Region (Southwest), Northeast Region (Northeast), and Southeast Region (Southeast) (Fig S3). Generally, the regions like CD Plain, CQ, Northeast SC, South SC were distributed within the SCB region, and could be regarded as the local regions. On the other hand, regions like Northwest, Southwest, Northeast, and Southeast were situated outside the SCB and air masses originating from these regions were considered to be a result of

regional transport. As Fig 9 shows, Chengdu was mainly affected by local regions, contributed to 46.8%. This implied that local emissions within the SCB were a significant contributor to the excessive O_3 levels in Chengdu. In contrast, the influence of the local region on O_3 levels in Chongqing was only 18.3%. Instead, the contribution outside the basin almost reached 50%, indicating that Chongqing was more susceptible to the influence of cross-regional transport. In general, the spatial disparity of O_3 pollution between Chongqing and Chengdu was decided by the changes in regional transport of O_3 and its precursors respectively with high and low contribution of non-local O_3-precursors to the two urban areas. This difference demonstrates that even the two major core cities located within the SCB exhibit distinct source contribution characteristics.
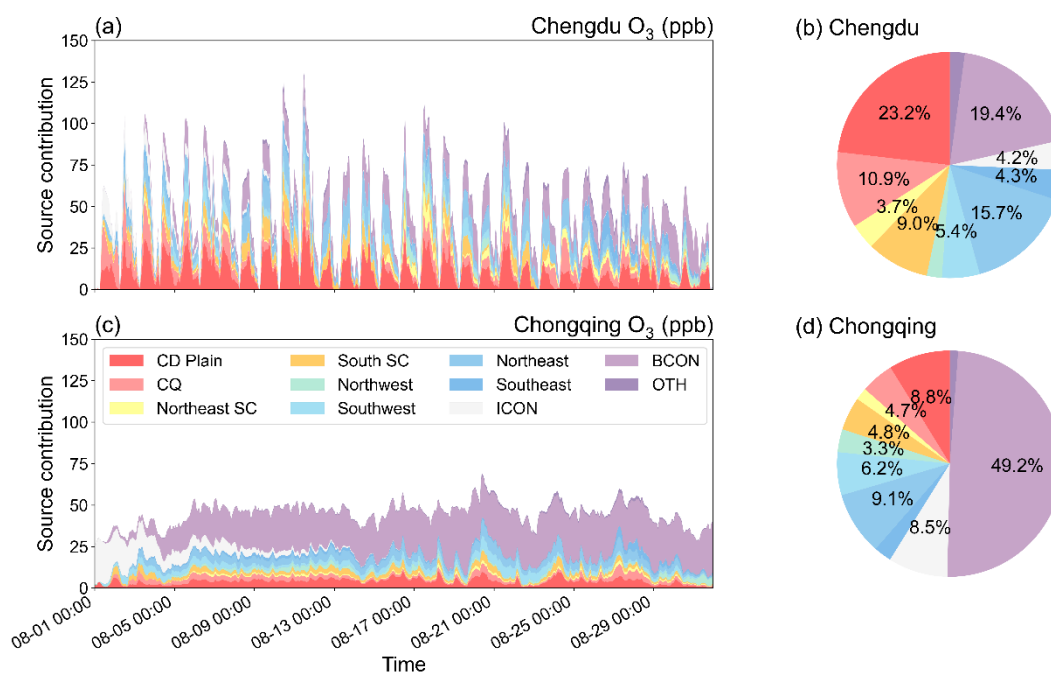
Fig 9 Source region's contribution to O_3 levels in Chengdu (a) Time series of O_3 contributions from each region. (b) Pie charts illustrating the percentage contributions of each region. (c) and (d) same as (a) and (b), but in Chongqing

Given that ambient O_3 concentrations are the integrated results of multiple processes, encompassing photochemical formation, deposition, and transport, we employed the Integrated Process Rate (IPR) tool within the CMAQ model to analyze the contributions of individual physical and chemical processes to O_3 levels. Here, we compared the contributions of different processes to O_3 during the peak period of heightened

photochemical reactions at 14:00 in the afternoon. As Fig. 10 shows, the process analysis results reveal distinct differences between the two cities. Specifically, in Chengdu, photochemical reactions took the lead in escalating O_3 levels (reaching 49.9 ppbv). This could be attributed to a combination of factors. On one hand, being limited to the local air masses, pollutants got accumulated and resulted in the increment of the atmospheric oxidizing capacity. On the other hand, under the influence of conducive meteorological conditions during heatwaves, the vigorous photochemical formation of O_3 was substantially enhanced, resulting in notable O_3 concentration increments. Compared to Chengdu, the contribution of photochemistry to O_3 in Chongqing was nearly half (29.2 ppbv). While both photochemical reactions and regional transport positively affected O_3 levels in Chongqing, the overall net accumulation of O_3 was notably lower in this city.
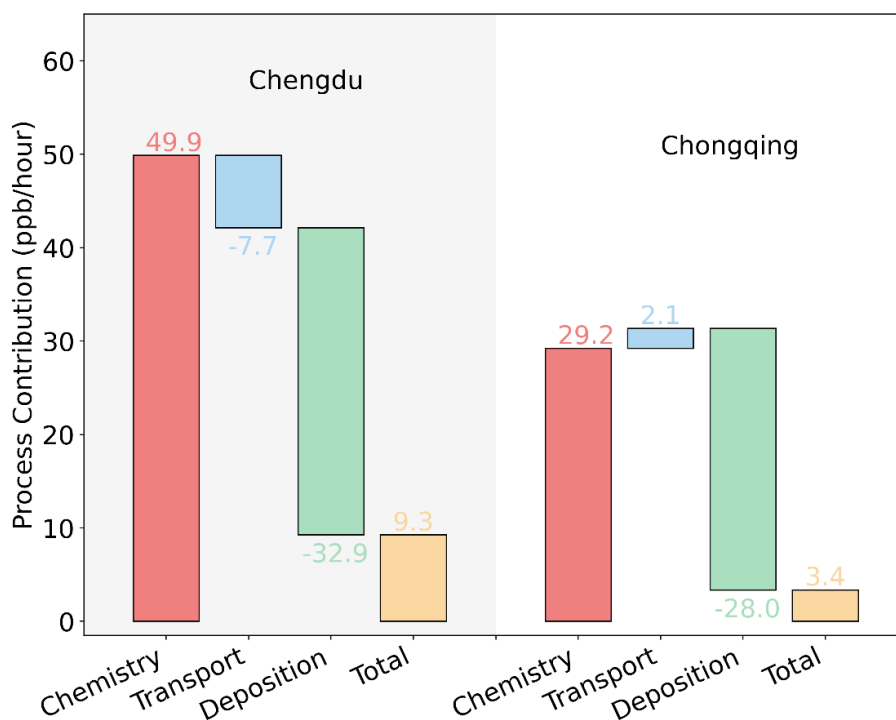
Fig 10 Averaged contributions of different process to O_3 concentrations at noon time (14:00) in Chengdu and Chongqing

4. Conclusion and implication

The unprecedented heatwave of August 2022 brought about significant divergence in O_3 levels between Chengdu and Chongqing, with exceeded

levels of O_3 appeared in the western SCB (Chengdu) but relatively lower concentrations in the eastern basin (Chongqing). Meteorological and precursor factors were assessed using a machine learning method, spotlighting high temperatures, intensive solar radiation, and overnight accumulative pollutants as key contributors to O_3 concentration. The interplay of isoprene, temperature, and O_3, alongside MEGAN calculations, underscored the intensified BVOCs emissions during heatwaves, highlighting the important role of meteorology-induced natural emissions. Interestingly, BVOCs emissions in Chongqing were nearly twice those in Chengdu; however, their contributions to O_3 concentrations were subdued. This discrepancy was attributed to the distinct responses of O_3-NO_x-VOCs sensitivity mechanisms. Chengdu exhibited sensitivity to VOCs, while Chongqing displayed a transitional sensitivity regime. Considering that China's previous emission reduction strategies have primarily focused on a nationwide NO_x reduction (driven by the need to control $PM_{2.5}$ pollution), it is important to recognize that a short-term reduction in NO_x can lead to an O_3 rebound in regions like Chengdu Plain. To achieve more precise pollution control, a strategy that combines VOCs as the primary focus with concurrent NO_x reductions would be more appropriate. In addition, the investigation into source region contributions revealed varying impacts of regional transport, even within the same basin. Chongqing was significantly influenced by cross-regional transport, whereas Chengdu was predominantly affected by local emissions.

These findings illuminate the complex interplay of meteorology, natural emissions, and anthropogenic sources during heatwaves, guiding the necessity of targeted pollution control measures. It is imperative to adopt emission control strategies that are customized according to regional or even local conditions, rather than enforcing uniform measures for the entire region. Given that O_3 pollution is not solely an in-situ problem but rather a regional issue, this concept extends beyond the SCB and is applicable to other urban clusters, such as the Beijing-Tianjin-Hebei region, the Yangtze River Delta region, the Pearl River Delta region, and developed regions in other countries. Future efforts are suggested to focus on regional coordinated and balanced control measures.

Author Contributions

F.Y. and N.W. designed the research. N.W. wrote the manuscript. N.W., D.Y., C.D., and M.H. contributed to the interpretation of the results. All the authors provided critical feedback and helped to improve the manuscript.

Competing Interests

The authors declare that they have no known competing financial interests or personal relationships that could have appeared to influence the work.

Acknowledgement

This study is supported by the National Key Research and Development Program (grant no.2023YFC3709304), the National Natural Science Foundation of China (No. 42175124 and No. 22276128), Science and Technology Department of Sichuan Province (23YFS0383), the Guangdong Basic and Applied Basic Research Foundation (Grant No. 2022A1515011753), the Fundamental Research Funds for the Central Universities (Grant No. YJ202313), and the Young Talent Support Project of Guangzhou Association for Science and Technology (Grant No. QT-2023-048). The authors also thank the Tsinghua University for compiling and sharing the MEIC emission inventory.

Financial Support

This study is funded by the National Key Research and Development Program (grant no. 2023YFC3709304), the National Natural Science Foundation of China (No. 42175124 and No. 22276128), Science and Technology Department of Sichuan Province (23YFS0383), the Guangdong Basic and Applied Basic Research Foundation (Grant No. 2022A1515011753), the Fundamental Research Funds for the Central Universities (Grant No. YJ202313), and the Young Talent Support Project of Guangzhou Association for Science and Technology (Grant No. QT-2023-048).

Reference

Bloss, C., Wagner, V., Jenkin, M. E., Volkamer, R., Bloss, W. J., Lee, J. D., Heard, D. E., Wirtz, K., Martin-Reviejo, M., Rea, G., Wenger, J. C., and Pilling, M. J.: Development of a detailed chemical mechanism (MCMv3.1) for the atmospheric oxidation of aromatic hydrocarbons, Atmos. Chem. Phys., 5, 641-664, 10.5194/acp-5-641-2005, 2005.

Cardelino, C. A. and Chameides, W. L.: An Observation-Based Model for Analyzing Ozone Precursor Relationships in the Urban Atmosphere, Journal of the Air & Waste Management Association, 45, 161-180, 10.1080/10473289.1995.10467356, 1995.

Chen, D., Zhou, L., Wang, C., Liu, H., Qiu, Y., Shi, G., Song, D., Tan, Q., and Yang, F.: Characteristics of ambient volatile organic compounds during spring O3 pollution episode in Chengdu, China, Journal of Environmental Sciences, 114, 115-125, 2022.

Daum, P. H., Kleinman, L. I., Springston, S. R., Nunnermacker, L., Lee, Y. N., Weinstein-Lloyd, J., Zheng, J., and Berkowitz, C. M.: A comparative study of O3 formation in the Houston urban and industrial plumes during the 2000 Texas Air Quality Study, Journal of Geophysical Research: Atmospheres, 108, 2003.

Ding, A., Huang, X., and Fu, C.: Air pollution and weather interaction in East Asia, in: Oxford Research Encyclopedia of Environmental Science, 2017.

Emberson, L., Ashmore, M., Murray, F., Kuylenstierna, J., Percy, K., Izuta, T., Zheng, Y., Shimizu, H., Sheu, B., and Liu, C.: Impacts of air pollutants on vegetation in developing countries, Water, Air, and Soil Pollution, 130, 107-118, 2001.

Hall, S. J., Matson, P. A., and Roth, P. M.: NOx emissions from soil: implications for air quality modeling in agricultural regions, Annual Review of Energy and the Environment, 21, 311-346, 1996.

Hu, J., Zhao, T., Liu, J., Cao, L., Wang, C., Li, Y., Shi, C., Tan, C., Sun, X., and Shu, Z.: Exploring the ozone pollution over the western Sichuan Basin, Southwest China: The impact of diurnal change in mountain-plains solenoid, Science of The Total Environment, 839, 156264, 2022.

Huang, J., Hartmann, H., Hellén, H., Wisthaler, A., Perreca, E., Weinhold, A., Ru¨cker, A., van Dam, N. M., Gershenzon, J., and Trumbore, S.: New perspectives on CO2, temperature, and light effects on BVOC emissions using online measurements by PTR-MS and cavity ring-down spectroscopy, Environmental science & technology, 52, 13811-13823, 2018.

Itahashi, S., Hayami, H., and Uno, I.: Comprehensive study of emission source contributions for tropospheric ozone formation over East Asia, Journal of Geophysical Research: Atmospheres, 120, 331-358, 2015.

Jacob, D. J.: Heterogeneous chemistry and tropospheric ozone, Atmospheric Environment, 34, 2131-2159, 2000.

Jenkin, M. E. and Clemitshaw, K. C.: Ozone and other secondary photochemical pollutants: chemical processes governing their formation in the planetary boundary layer, Atmospheric Environment, 34, 2499-2527, 2000.

Jenkin, M. E., Saunders, S. M., and Pilling, M. J.: The tropospheric degradation of volatile organic compounds: a protocol for mechanism development, Atmospheric Environment, 31, 81-104, https://doi.org/10.1016/S1352-2310(96)00105-7, 1997.

Jenkin, M. E., Young, J. C., and Rickard, A. R.: The MCM v3.3.1 degradation scheme for isoprene, Atmos. Chem. Phys., 15, 11433-11459, 10.5194/acp-15-11433-2015, 2015.

Jenkin, M. E., Saunders, S. M., Wagner, V., and Pilling, M. J.: Protocol for the development of the Master Chemical Mechanism, MCM v3 (Part B): tropospheric degradation of aromatic volatile organic compounds, Atmos. Chem. Phys., 3, 181-193, 10.5194/acp-3-181-2003, 2003.

Krupa, S. V. and Kickert, R. N.: The greenhouse effect: impacts of ultraviolet-B (UV-B) radiation, carbon dioxide (CO2), and ozone (O3) on vegetation, Environmental Pollution, 61, 263-393, 1989.

Kwok, R. H., Napelenok, S. L., and Baker, K. R.: Implementation and evaluation of PM2. 5 source contribution analysis in a photochemical model, Atmospheric Environment, 80, 398-407, 2013.

Lei, Y., Wu, K., Zhang, X., Kang, P., Du, Y., Yang, F., Fan, J., and Hou, J.: Role of meteorology-driven regional transport on O3 pollution over the Chengdu Plain, southwestern China, Atmospheric Research, 285, 106619, 2023.

Lelieveld, J. and Dentener, F. J.: What controls tropospheric ozone?, Journal of Geophysical Research: Atmospheres, 105, 3531-3551, 10.1029/1999jd901011, 2000.

Lu, X., Zhang, L., and Shen, L.: Meteorology and Climate Influences on Tropospheric Ozone: a Review of Natural Sources, Chemistry, and Transport Patterns, Current Pollution Reports, 5, 238-260, 10.1007/s40726-019-00118-3, 2019.

McElroy, M. B., Salawitch, R. J., and Wofsy, S. C.: Antarctic O3: Chemical mechanisms for the spring decrease, Geophysical research letters, 13, 1296-1299, 1986.

Meng, X., Jiang, J., Chen, T., Zhang, Z., Lu, B., Liu, C., Xue, L., Chen, J., Herrmann, H., and Li, X.: Chemical drivers of ozone change in extreme temperatures in eastern China, Science of The Total Environment, 874, 162424, https://doi.org/10.1016/j.scitotenv.2023.162424, 2023.

Napelenok, S., Cohan, D., Odman, M. T., and Tonse, S.: Extension and evaluation of sensitivity analysis capabilities in a photochemical model, Environmental Modelling & Software, 23, 994-999, 2008.

Potosnak, M. J., LeStourgeon, L., Pallardy, S. G., Hosman, K. P., Gu, L., Karl, T., Geron, C., and Guenther, A. B.: Observed and modeled ecosystem isoprene fluxes from an oak-dominated temperate forest and the influence of drought stress, Atmospheric Environment, 84, 314-322, 2014.

Qiao, X., Guo, H., Wang, P., Tang, Y., Ying, Q., Zhao, X., Deng, W., and Zhang, H.: Fine particulate matter and ozone pollution in the 18 cities of the Sichuan Basin in southwestern China: model performance and characteristics, Aerosol and Air Quality Research, 19, 2308-2319, 2019.

Saunders, S. M., Jenkin, M. E., Derwent, R. G., and Pilling, M. J.: Protocol for the development of the Master Chemical Mechanism, MCM v3 (Part A): tropospheric degradation of non-aromatic volatile organic compounds, Atmos. Chem. Phys., 3, 161-180, 10.5194/acp-3-161-2003, 2003.

Saunier, A., Ormeño, E., Boissard, C., Wortham, H., Temime-Roussel, B., Lecareux, C., Armengaud, A., and Fernandez, C.: Effect of mid-term drought on Quercus pubescens BVOCs' emission seasonality and their dependency on light and/or temperature, Atmospheric Chemistry and Physics, 17, 7555-7566, 2017.

Schwela, D.: Air pollution and health in urban areas, Reviews on environmental health, 15, 13-42, 2000.

Shu, Z., Zhao, T., Liu, Y., Zhang, L., Ma, X., Kuang, X., Li, Y., Huo, Z., Ding, Q., and Sun, X.: Impact of deep basin terrain on PM2. 5 distribution and its seasonality over the Sichuan Basin, Southwest China, Environmental Pollution, 300, 118944, 2022.

Wang, H., Lu, X., Seco, R., Stavrakou, T., Karl, T., Jiang, X., Gu, L., and Guenther, A. B.: Modeling Isoprene Emission Response to Drought and Heatwaves Within MEGAN Using Evapotranspiration Data and by Coupling With the Community Land Model, Journal of advances in modeling earth systems, 14, e2022MS003174, 10.1029/2022MS003174, 2022a.

Wang, N., Guo, H., Jiang, F., Ling, Z., and Wang, T.: Simulation of ozone formation at different elevations in mountainous area of Hong Kong using WRF-CMAQ model, Science of the total environment, 505, 939-951, 2015.

Wang, N., Huang, X., Xu, J., Wang, T., Tan, Z.-m., and Ding, A.: Typhoon-boosted biogenic emission aggravates cross-regional ozone pollution in China, Science Advances, 8, eabl6166, 2022b.

Wang, P., Qiao, X., and Zhang, H.: Modeling PM2. 5 and O3 with aerosol feedbacks using WRF/Chem over the Sichuan Basin, southwestern China, Chemosphere, 254, 126735, 2020.

Wang, T., Xue, L., Brimblecombe, P., Lam, Y. F., Li, L., and Zhang, L.: Ozone pollution in China: A review of concentrations, meteorological influences, chemical precursors, and effects, Science of

811 the Total Environment, 575, 1582‑1596, 2017.

812 Xiao, Q., Geng, G., Xue, T., Liu, S., Cai, C., He, K., and Zhang, Q.: Tracking PM2. 5 and O3 pollution
813 and the related health burden in China 2013–2020, Environmental science & technology, 56, 6922‑
814 6932, 2021.

815 Xue, L., Wang, T., Wang, X., Blake, D. R., Gao, J., Nie, W., Gao, R., Gao, X., Xu, Z., Ding, A., Huang,
816 Y., Lee, S., Chen, Y., Wang, S., Chai, F., Zhang, Q., and Wang, W.: On the use of an explicit chemical
817 mechanism to dissect peroxy acetyl nitrate formation, Environ Pollut, 195, 39‑47,
818 10.1016/j.envpol.2014.08.005, 2014.

819 Zhang, Y., Sun, J., Zheng, P., Chen, T., Liu, Y., Han, G., Simpson, I. J., Wang, X., Blake, D. R., Li, Z.,
820 Yang, X., Qi, Y., Wang, Q., Wang, W., and Xue, L.: Observations of C-1-C-5 alkyl nitrates in the
821 Yellow River Delta, northern China: Effects of biomass burning and oil field emissions, Science of
822 the Total Environment, 656, 129‑139, 10.1016/j.scitotenv.2018.11.208, 2019.

823 Zhao, S., Yu, Y., Yin, D., Qin, D., He, J., and Dong, L.: Spatial patterns and temporal variations of six
824 criteria air pollutants during 2015 to 2017 in the city clusters of Sichuan Basin, China, Science of
825 the Total Environment, 624, 540‑557, 2018.

826 Zhou, Z., Tan, Q., Deng, Y., Song, D., Wu, K., Zhou, X., Huang, F., Zeng, W., and Lu, C.: Compilation
827 of emission inventory and source profile database for volatile organic compounds: A case study
828 for Sichuan, China, Atmospheric Pollution Research, 11, 105‑116, 2020.

829 Zhu, J. X., Cheng, H. R., Peng, J., Zeng, P., Wang, Z. W., Lyu, X. P., and Guo, H.: O-3 photochemistry
830 on O-3 episode days and non-O-3 episode days in Wuhan, Central China, Atmospheric
831 Environment, 223, 10.1016/j.atmosenv.2019.117236, 2020.

832